Tectonophysics 634 (2014) 139–155

Contents lists available at ScienceDirect

Tectonophysics

journal homepage: www.elsevier.com/locate/tecto

Seismicity change revealed by ETAS, PI, and Z-value methods: A case study of the 2013 Nantou, Taiwan earthquake

Masashi Kawamura [a,*], Chien-chih Chen [b], Yih-Min Wu [a]

[a] Department of Geosciences, National Taiwan University, No. 1, Sec. 4, Roosevelt Road, Taipei 10617, Taiwan
[b] Department of Earth Sciences and Graduate Institute of Geophysics, National Central University, Taiwan

ARTICLE INFO

Article history:
Received 14 October 2013
Received in revised form 20 July 2014
Accepted 23 July 2014
Available online 4 August 2014

Keywords:
Pattern informatics method
ZMAP
ETAS model
Seismic quiescence
Preseismic slip
The Nantou earthquake

ABSTRACT

On Mar. 27, 2013, a M_L6.2 earthquake occurred in the Nantou area of central Taiwan, which caused one death and nearly 90 injured. Two months later, another M_L6.3 earthquake struck the same region on June 2, 2013, the epicenter of which is close to the March M_L6.2 earthquake. Seismicity is a sensitive indicator of stress rate and inelastic deformation process in crust. Therefore, examination of temporal changes in seismicity is important to understand the preparatory processes of damaging inland earthquakes. In this study, we applied the Epidemic-Type Aftershock-Sequences model (ETAS model) to the earthquake data covering broader Taiwan region, which is maintained by the Central Weather Bureau (CWB) of Taiwan, to investigate precursory temporal changes in seismicity for the M_L6.2 Nantou earthquake. We regard the March M_L6.2 and June M_L6.3 earthquakes as an event sequence and especially focus on temporal changes in seismicity prior to the M_L6.2 event. Application of more than one model to an earthquake catalog would be informative in elucidating the relationships between seismicity precursors and the preparatory processes of large earthquakes. Based on this motivation, we further applied two different approaches: the pattern informatics (PI) method and the ZMAP method, which is a gridding technique based on the standard deviate (Z-value) test to the same earthquake data of CWB. As a result, we found that the epicenter of the 2013 M_L6.2 Nantou earthquake was surrounded by three main seismic quiescence regions prior to its occurrence. The assumption that this is due to precursory slip (stress drop) on fault plane or its deeper extent of the M_L6.2 Nantou earthquake is supported by previous researches based on seismicity data, geodedic data, and numerical simulations using rate- and state-dependent friction laws.

1. Introduction

A M_L6.2 earthquake occurred at a depth of 15.4 km in Nantou, central Taiwan, on Mar. 27, 2013, which caused one death and nearly 90 injured. Two months later, another same-class (M_L6.3) earthquake hit the same region on June 2, 2013, the epicenter of which is close to the March M_L6.2 earthquake (Chuang et al., 2013). Like these cases, even M6-class earthquakes can inflict large damage depending on various factors such as their epicenters, depths, and focal mechanisms. Thus it is an urgent issue to reveal the preparatory processes of large earthquakes. Seismicity is a sensitive indicator of stress variation over an area under investigation (Kato et al., 1997; Ma et al., 2005; Stein, 1999; Toda et al., 2002). Therefore, it would be a useful approach to investigate temporal changes in seismicity for the occurrence of a large earthquake. This is supported by past researches in which seismic quiescence, seismic activation, or their migrations prior to large earthquakes was reported in various regions (Bansal and Ogata, 2013; Bowman and King, 2001; Bowman et al., 1998; Bufe and Varnes, 1993; Bufe et al., 1994; Jaume and Sykes, 1999; Karakaisis et al., 2002; Kawamura and Chen, 2013; Kawamura et al., 2013, 2014; Mogi, 1969; Papazachos et al., 2010; Resenberg and Matthews, 1988; Sykes and Jaume, 1990; Wu et al., 2011; Wyss and Wiemer, 1997).

Taiwan is one of high seismicity regions that have historically been struck by large earthquakes. The most recent and destructive one is the 1999 Chi-Chi earthquake (M_L7.3), which occurred near the Chelungpu fault in the western part of central Taiwan on Sep. 20, 1999 and caused many casualties and traffic disruptions. Its precursory seismicity change has retrospectively been investigated by many researchers (Chen, 2003; Chen et al., 2005; Kawamura and Chen, 2013; Wu and Chen, 2007; Wu and Chiao, 2006; Wu et al., 2008a). Chen (2003) found that seismicity of moderate-sized earthquakes had been activated prior to the Chi-Chi event by focusing on the temporal change in the Gutenberg–Richter scaling distribution; Chen et al. (2005) identified anomalous seismicity in the source area of the Chi-Chi earthquake prior to its occurrence using the pattern informatics (PI) method (Chen et al., 2006; Holliday et al., 2005, 2006; Rundle et al., 2000; Tiampo et al., 2002a, 2002b; Wu et al., 2008a); Wu and Chiao (2006) showed that a broader region around the source area of the Chi-Chi earthquake had revealed seismic quiescence before the Chi-Chi earthquake with the ZMAP analysis (Console et al., 2000; Habermann, 1988; Habermann and Wyss, 1984; Wiemer and Wyss, 1994); Wu

* Corresponding author. Tel.: +886 2 3366 4956x310; fax: +886 2 2363 9154.
E-mail addresses: mkawamu@ntu.edu.tw, mkawa76@msn.com (M. Kawamura).

http://dx.doi.org/10.1016/j.tecto.2014.07.028
0040-1951/

and Chen (2007) indicated the emergence of seismic quiescence over a broad region of Eastern Taiwan and seismic activation near the epicenter of the Chi-Chi earthquake with the same ZMAP analysis but using a longer earthquake catalog including both before and after the Chi-Chi earthquake. Kawamura and Chen (2013) indicated the existence of seismic quiescence over broader regions of Taiwan and that inland areas near the epicenter of the Chi-Chi earthquake exhibited seismic activation during the period from Jan. 1, 1998 to Sep. 20, 1999 right before the Chi-Chi event by applying the Epidemic-Type Aftershock-Sequences (ETAS) model (Ogata, 1988, 1992, 1999) to the earthquake catalog of the Taiwan region. These reports imply that there exists anomalous seismicity change associated with the Chi-Chi earthquake both near its epicenter and over broader regions of Taiwan and that the ETAS model, the PI method, and the ZMAP analysis have the capability of detecting anomalous seismicity in Taiwan region.

To further understand the preparatory process of a large earthquake and its associated seismicity change, we investigated the spatial distribution of seismicity change during a time span prior to the 2013 M_L6.2 Nantou earthquake. Because the magnitude of the earthquake is nearly 6, or much less than 7 and 8, this study would provide a reference for the occurrence (or non-occurrence) of seismicity change prior to M6-class earthquake. On the basis of previous successful applications of statistical models, we applied the ETAS model to the earthquake data covering broader Taiwan region, which is maintained by the Central Weather Bureau (CWB) of Taiwan. In addition, applications of different models to the same dataset of the CWB are expected to enhance the reliability of the result obtained: the spatial distribution of seismic quiescence and activation prior to the M_L6.2 Nantou earthquake. We thus further applied two different statistical approaches of the PI method and the ZMAP analysis to the CWB earthquake catalog data with the same time spans prior to the M_L6.2 Nantou earthquake. In this study, we regarded the March M_L6.2 and June M_L6.3 earthquakes as an event sequence and only focus on temporal changes in seismicity prior to the March M_L6.2 event.

In Section 2, we introduce the ETAS, PI, and ZMAP analyses. In Section 3, we show that the epicenter of the 2013 M_L6.2 Nantou earthquake is surrounded by regions with seismic quiescence (the ETAS and ZMAP analyses) or large seismicity changes (the PI method). In Section 4, we compare the spatial distribution of seismic quiescence and activation obtained using the ETAS analysis with those obtained using the PI and ZMAP analyses to evaluate precursory temporal changes in seismicity for the M_L6.2 Nantou earthquake.

2. Data and methodology

We used the CWB earthquake catalog data which spanning the time period of 1994–2013 for the ETAS, PI, and ZMAP analyses. Fig. 1 shows the epicenter distribution of earthquakes with local magnitude (M_L) greater than or equal to 3.0 at depths of 0–30 km during 1990–2013. Fault traces (Central Geological Survey, 2010) and focal mechanism solutions for the Mar. 27, 2013 M_L6.2 event and the Jun. 2, 2013 M_L6.3 event together with trenches around Taiwan region are also denoted in Fig. 1. For ETAS analysis, we used cutoff magnitude of 2.4 based on the result of Mignan et al. (2011) and the maps of magnitude completeness (Mc) (Fig. 2), which was obtained by the method of Wiemer and Wyss (2000). To calculate Mc for each grid cell, we used 400 earthquakes at depths of 0–30 km. The Mc's for all grid cells are smaller than or equal to 2.4 (2.0 for a large part of inland Taiwan) except for 2.5 or 2.6 for four bottom grid cells (121.125°, 121.375°, 121.625°, 121.875°) in panel (a) and 2.5 for a bottom grid cell (120.625°) in panel (c). These grid cells are out of consideration in this study. For the ETAS, PI, and ZMAP methods, we chose the earthquakes at depths shallower than 30 km. The depth of 30 km corresponds to the thickness of the crustal seismogenic zone in this region.

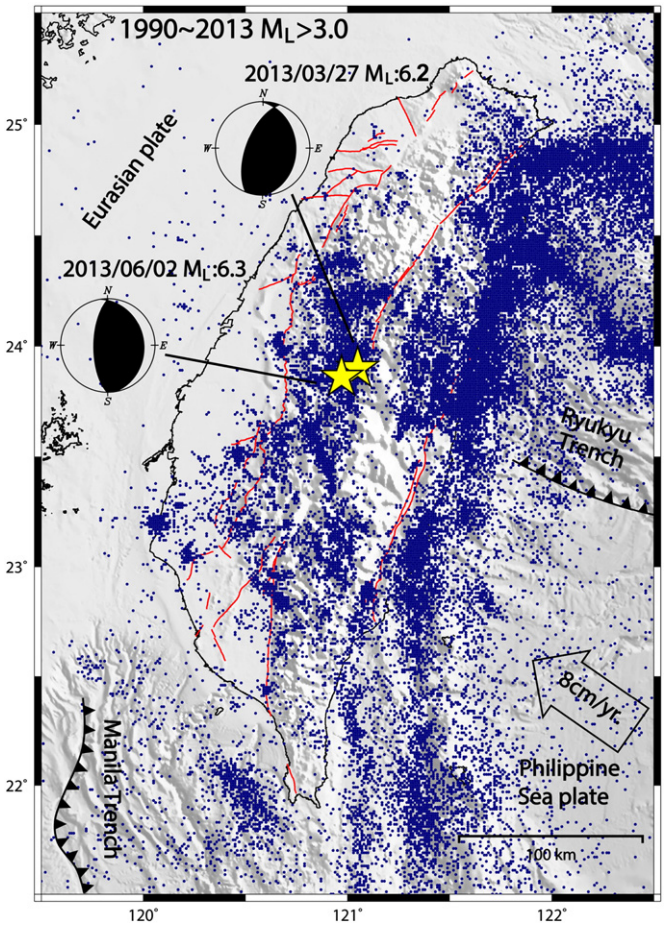

Fig. 1. Seismic activity in and around Taiwan region. Blue dots show the epicenters of earthquakes with local magnitude (M_L) greater than or equal to 3.0 at depths of 0–30 km during 1990–2013. The red lines in inland Taiwan and the black lines with closed triangles in ocean region correspond to fault traces and trenches, respectively. The yellow stars with focal mechanism solutions denote the epicenters of the March 2013 Nantou earthquake (M_L6.2) and June 2013 Nantou earthquake (M_L6.3).

2.1. The ETAS analysis

The ETAS model (Ogata, 1988, 1992, 1999) is a point process model and the seismicity rate λ (unit: events/day) is expressed as follows:

$$\lambda(t) = \mu + \sum_{t_j<t} K \exp\left\{\alpha\left(M_j - M_c\right)\right\} \Big/ \left(t - t_j + c\right)^p, \tag{1}$$

where μ is background seismicity rate, t_j and M_j is time and magnitude of j-th earthquake, M_c is cutoff magnitude, K is a constant related to aftershock productivity, α is a constant representing the efficiency of earthquake with a magnitude of M_j, c is a constant for adjusting time axis, p is a constant reflecting the temporal attenuation of seismicity. The cumulative number of earthquakes at time t since t_s can be expressed as below:

$$\begin{aligned} \Lambda(t) = \int_{t_s}^{t} \lambda(s)ds &= \mu(t - t_s) \\ &+ K \sum_{t_j<t} \exp\left\{\alpha\left(M_j - M_c\right)\right\} \left\{c^{1-p} - \left(t - t_j + c\right)^{1-p}\right\} \Big/ (p-1), \end{aligned} \tag{2}$$

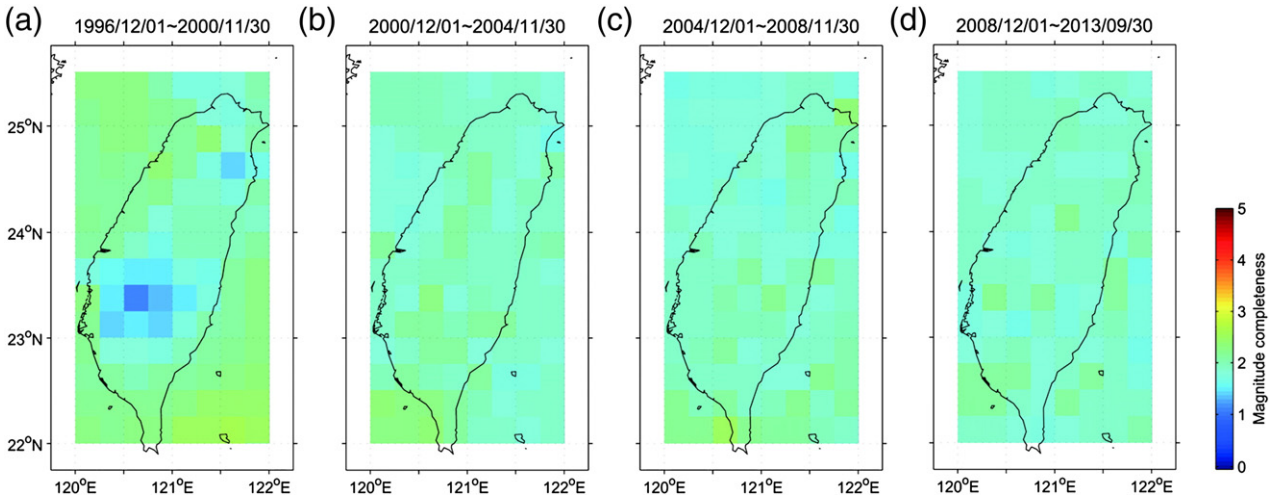

Fig. 2. Magnitude completeness (Mc) obtained by the method of Wiemer and Wyss (2000) for four consecutive time periods as shown on top of panels. To calculate Mc for each grid cell, we used 400 earthquakes at depths of 0–30 km. The Mc's for all grid cells are smaller than or equal to 2.4 (2.0 for a large part of inland region) except for 2.5 or 2.6 for four bottom grid cells (121.125°, 121.375°, 121.625°, 121.875°) in panel (a) and 2.5 for a bottom grid cell (120.625°) in panel (c). These grid cells are out of consideration in this study.

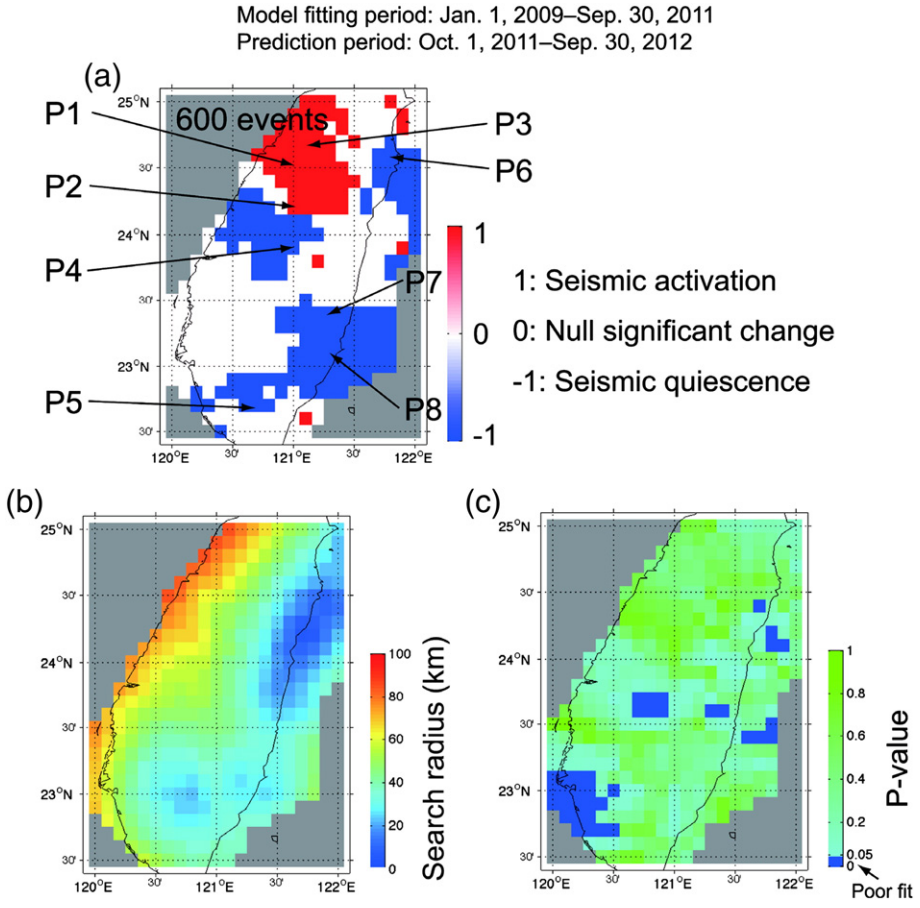

Fig. 3. (a) ETAS map with a cutoff magnitude of 2.4: Spatial distribution showing three patterns of temporal changes in seismicy (seismic quiescence, seismic activation, and null significant change) for circular areas centered at respective calculation grid cells. Grid cells colored blue show seismic quiescence for the prediction period (Oct. 1, 2011–Sep. 30, 2012) relative to the target period (model fitting period: Jan. 1, 2009–Sep. 30, 2011). Those colored red denote seismic activation. Those colored white correspond to null significant temporal changes in seismicity. The label of "600 events" means the total collected number of events used for ETAS calculation for each calculation grid cell. (b) Event search radius map: Spatial distribution showing the radii within which 600 events are collected for making the ETAS map. (c) P-value map, which is obtained by calculating Kolmogorov–Smirnov statistics showing the goodness of model fit.

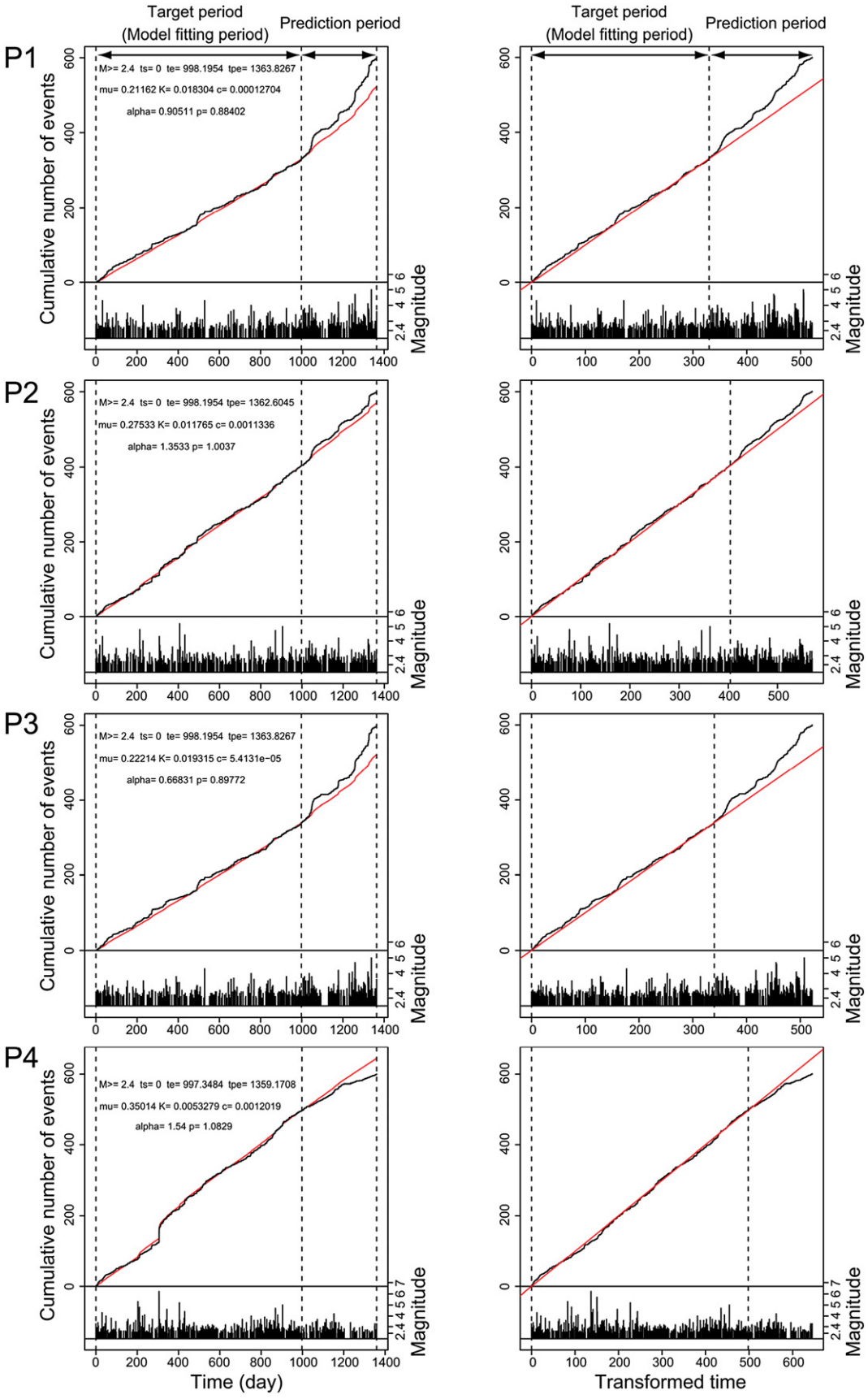

Fig. 4. The plots of cumulative number of events against time (left panels) and transformed time (right panels) for circular areas centered at calculation grid cells of P1 to P8, the locations of which are shown in Fig. 3a.

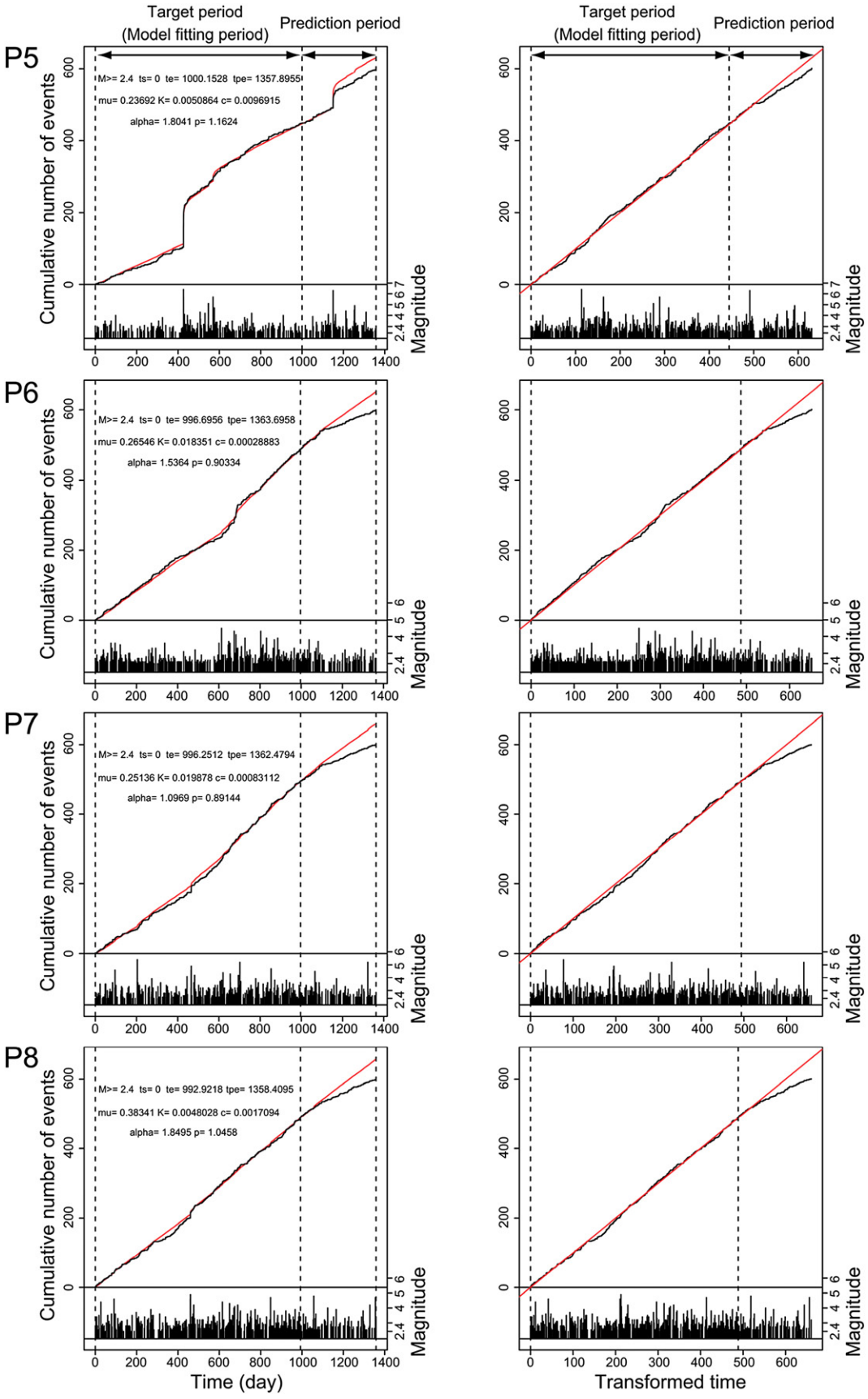

Fig. 4 (*continued*).

where $\tau_j = \Lambda(t_j)$ is transformed time, which is equivalent to theoretical cumulative number of earthquakes until the occurrence time t_j of j-th earthquake. Parameters μ, K, c, α, and p are can be estimated by maximizing the following log likelihood function (Ogata, 1988, 1992, 1999):

$$\log L = \sum_{t_s<t_j<t_e} \log\lambda\left(t_j\right) - \int_{t_s}^{t_e} \lambda(t)dt. \quad (3)$$

where t_s and t_e show the beginning and end times of model-fitting period, respectively. Although our ETAS analysis procedure is as explained below, the reader can also refer to the detailed flowchart shown in Fig. 1 of Kawamura and Chen (2013). After Taiwan region is divided into grid cells with a dimension of 0.1° × 0.1°, the ETAS model is applied to fit the curve of cumulative event number for circular region centered at each calculation grid cell for "target (model-fitting) period". Total number of events collected was set constant (600 events) for every calculation grid cell. The target period is discriminated from the subsequent "prediction period" in which the occurrence of anomalous seismicity change is assessed. In this study, the target periods were set to Jan. 1, 2009–Sep. 30, 2011 (Figs. 3 and 4), Mar. 1, 2007–Feb. 29, 2012 (Figs. 5 and 6), Mar. 1, 2008–Feb. 29, 2012 (Figs. 7 and 8), and Mar. 1, 2009–Feb. 29, 2012 (Figs. 9 and 10); the corresponding prediction periods were set as Oct. 1, 2011–Sep. 30, 2012 (Figs. 3 and 4) and Mar 1, 2012–Feb. 28, 2013 (Figs. 5–10). This assessment is based on statistical tests a) (statistics Z_A) and b) (statistics Z_B) with a confidence level of 95% as explained in Appendix A or Kawamura and Chen (2013). Statistics Z_A assesses the significance of change in mean difference between modeled and actual cumulative numbers of earthquakes for the first half and the latter half of the prediction period; Statistics Z_B assesses the significance of difference between the numbers of local transformed-time windows for seismic quiescence and seismic activation in the prediction period. By assessing seismicity changes for all grid cells, the ETAS map, or the spatial distribution of seismicity change is obtained.

2.2. The PI method

The PI method was originally developed based on the concept of pattern dynamics (Rundle et al., 2000), in which stress is a space–time state variable in a system of true deterministic dynamics. Because direct observation of stress change is, however, difficult, we instead focus on seismicity, which can be regarded as an indicator of stress, as a space–time state variable of the pattern dynamics to investigate the change in an earthquake system. We applied the PI method as follows. (1) The target region is set and divided into 0.1° × 0.1° grid cells and active grid cells ranking in the top 30% are considered. (2) The seismic intensity change $\Delta I(t_b,t_1,t_2)$ is calculated for a calculation grid cell for the two different target time periods (or change intervals: t_1–t_2): Oct. 1, 2011–Sep. 30, 2012 and Mar. 1, 2012–Feb. 28, 2013. This calculated change is used to obtain an index defined as PI value, which likely represents the probability of earthquake occurrence after t_2. Seismic intensity $I(t_b,t)$ is defined as the number of earthquakes per day within a square area that includes the calculation grid cell and its eight neighboring cells, averaged over the time period between a reference time t_b (where $t_0 < t_b < t_1$ and t_0 = Nov. 30, 1996) and t. To obtain seismic intensity change, seismic intensities $I(t_b,t_1)$ and $I(t_b,t_2)$ for the

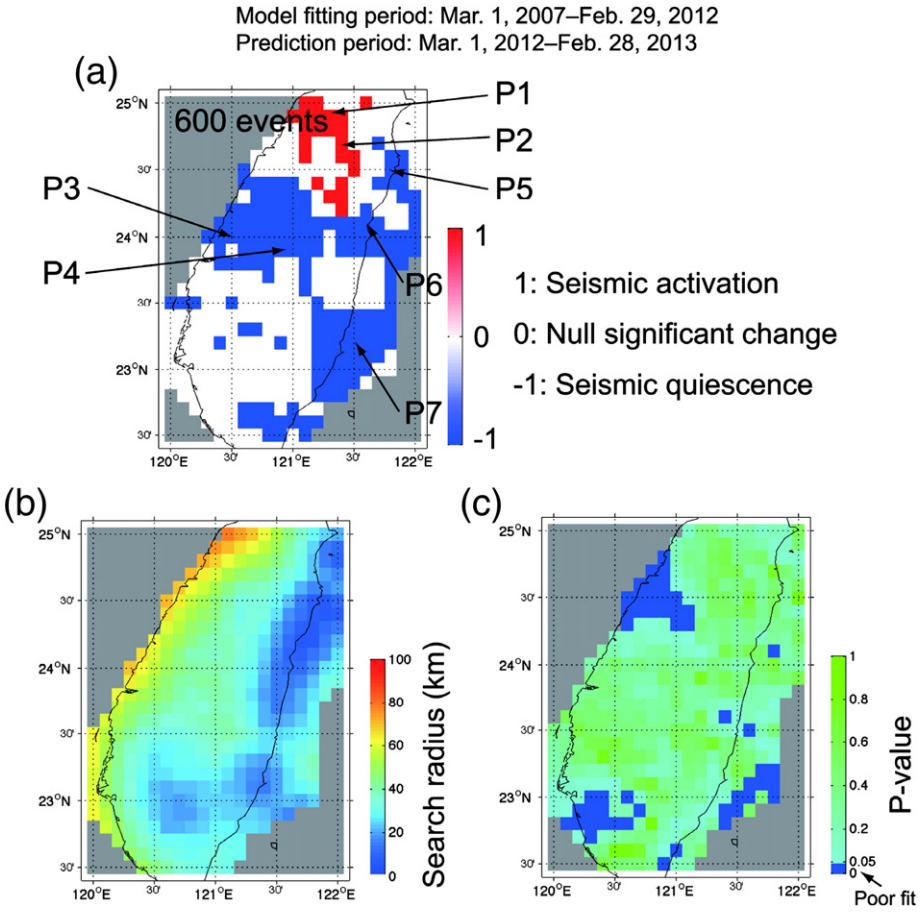

Fig. 5. As in Fig. 3, but for the target period of Mar. 1, 2007–Feb. 29, 2012 and the prediction period of Mar. 1, 2012–Feb. 28, 2013.

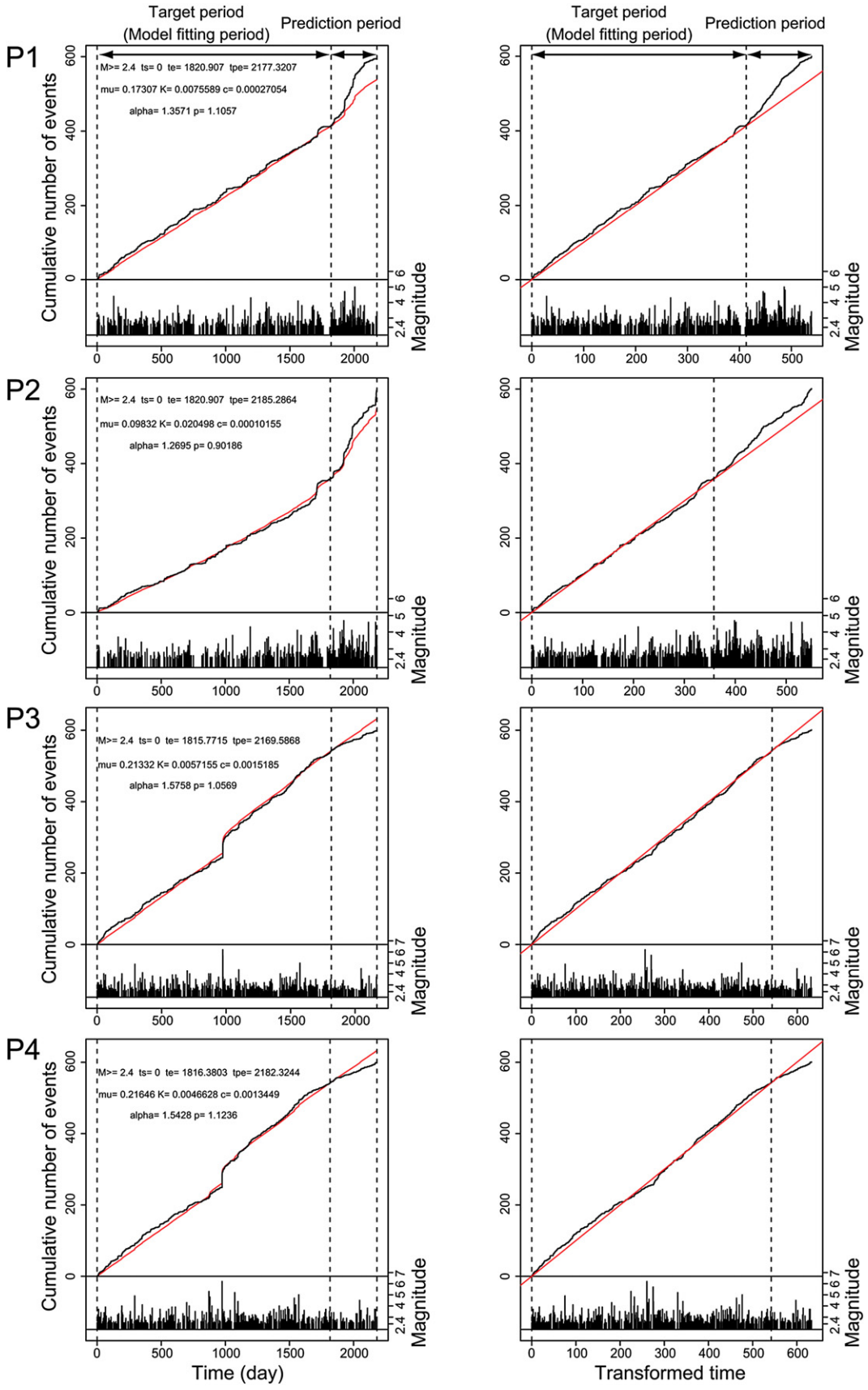

Fig. 6. As in Fig. 4, but for the target period of Mar. 1, 2007–Feb. 29, 2012 and the prediction period of Mar. 1, 2012–Feb. 28, 2013; the locations of P1 to P7 are shown in Fig. 5a.

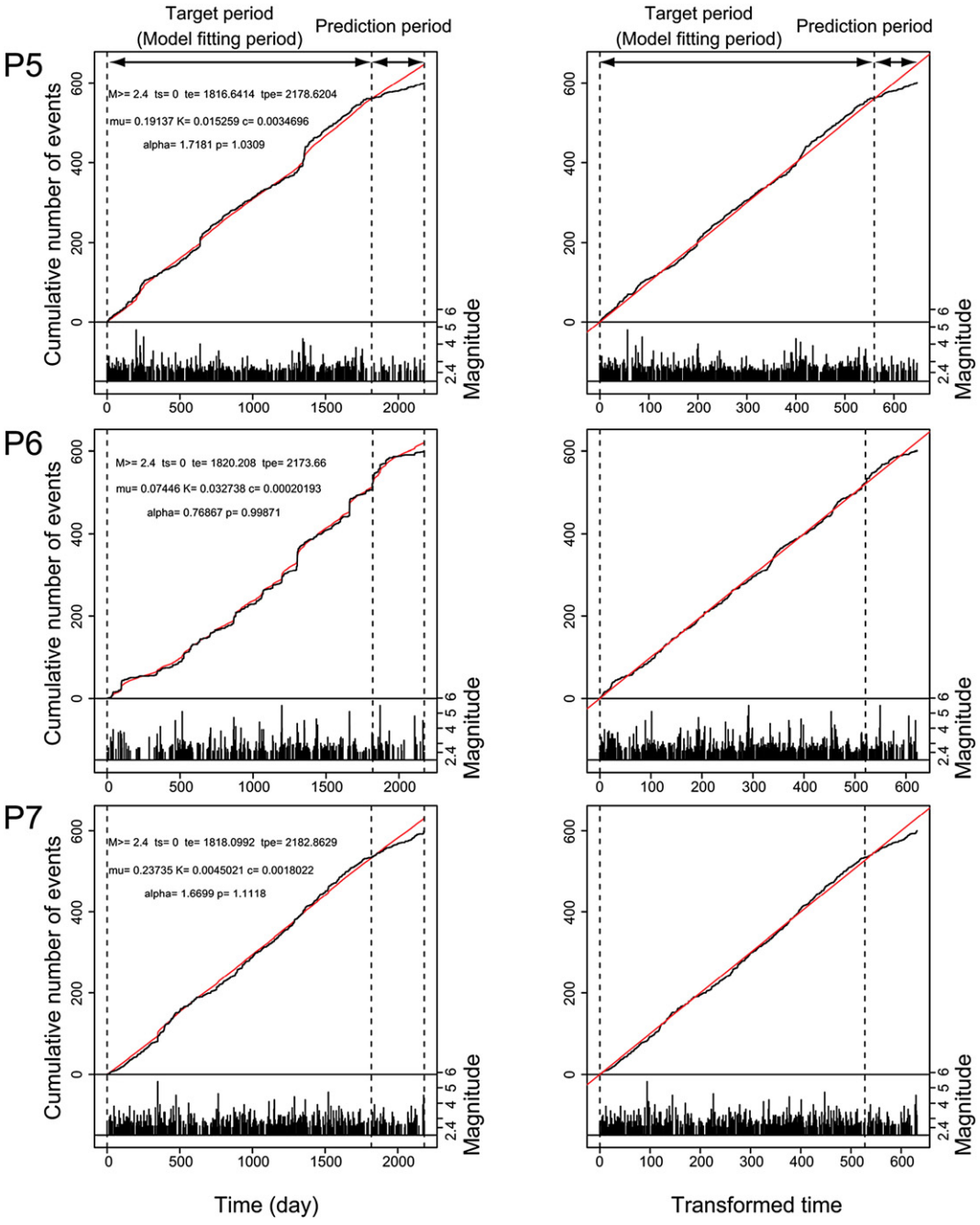

Fig. 6 (*continued*).

calculation grid cell are calculated for the corresponding time periods (i.e. $t_b - t_1$ and $t_b - t_2$, respectively). Then, seismic intensity change is calculated as follows: $\Delta I(t_b,t_1,t_2) = I(t_b,t_2) - I(t_b,t_1)$. (3) This process (2) is repeated to obtain seismic intensity changes for all grid cells. (4) Seismic intensities $I(t_b,t_1)$ and $I(t_b,t_2)$ are calculated again by shifting t_b from t_0 to t_1; then, seismic intensity change $\Delta I(t_b,t_1,t_2)$ is calculated for each calculation grid cell. (5) $\Delta I(t_b,t_1,t_2)$ for each calculation grid cell is normalized temporally (as to t_b) by subtracting its temporal mean and dividing by its temporal standard deviation. (6) Additionally, $\Delta I(t_b,t_1, t_2)$ is normalized spatially by subtracting its spatial mean and then dividing by its spatial standard deviation for every value of t_b. The spatiotemporally normalized seismic intensity change $\Delta\hat{I}(t_b,t_1,t_2)$ can then be obtained and most of the effects of random fluctuation in seismic intensity change and background seismic intensity change are eliminated. (7) The preseismic change $\Delta\hat{I}(t_b,t_1,t_2)$ can be seismic quiescence, seismic activation, or even both; therefore, $\Delta\hat{I}(t_b,t_1,t_2)$ may be negative or positive. To incorporate all preseismic change and reduce the fluctuation of random noise, we take the absolute value of the spatiotemporally normalized seismic intensity $|\Delta\hat{I}(t_b,t_1,t_2)|$ and average this absolute value over all values of t_b to obtain $\overline{\left|\Delta\hat{I}(t_b,t_1,t_2)\right|}$. (8) Then, the probability of earthquake occurrence $P(t_1,t_2)$ is defined as $\overline{\left|\Delta\hat{I}(t_b,t_1,t_2)\right|}^2$ and the average probability as the spatial mean μ_p of $P(t_1,t_2)$. The probability of earthquake occurrence relative to the background mean, $\Delta P(t_1,t_2) \equiv \overline{\left|\Delta\hat{I}(t_b,t_1,t_2)\right|}^2 - \mu_p$, is further divided by the spatial maximum (ΔP_{max}); thus obtained $\Delta P/\Delta P_{max}$ is defined as PI value. (9) The common logarithm of PI value is color coded and plotted on PI map.

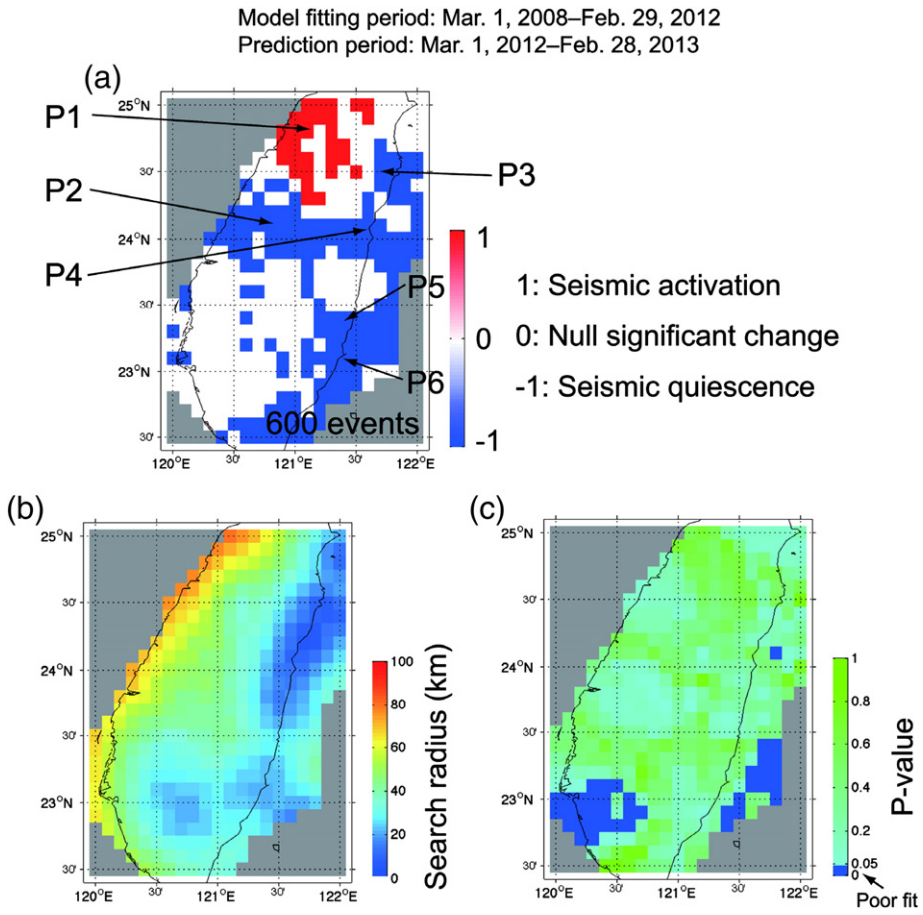

Fig. 7. As in Fig. 3, but for the target period of Mar. 1, 2008–Feb. 29, 2012 and the prediction period of Mar. 1, 2012–Feb. 28, 2013.

2.3. The ZMAP calculation

The ZMAP method (Wiemer and Wyss, 1994; Wu and Chiao, 2006; Katsumata, 2011; Wu et al., 2008b) creates an image of the significance of seismicity rate changes in space and time by the equation,

$$Z = \left(R_{bg} - R_{cal}\right) \Big/ \sqrt{\sigma_{bg}/n_{bg} + \sigma_{cal}/n_{cal}}, \tag{4}$$

where R_{bg} and R_{cal} are the mean seismicity rates for background and calculation periods, respectively; σ_{bg} and σ_{cal} are the standard deviations of seismicity rate for respective periods; n_{bg} and n_{cal} are the numbers of events for respective periods. In this study, two different background periods were defined as follows: Jan. 1, 1994–Sep. 30, 2012 and Jan. 1, 1994–Feb. 28, 2013. Their corresponding calculation periods were set to Oct. 1, 2011–Sep. 30, 2012 and Mar. 1, 2012–Feb. 28, 2013, respectively. The intervals of grid cells were set to 0.2° × 0.2° by taking the location errors of hypocenters into account.

3. Results

In this study, we focus on inland Taiwan region and its periphery to evaluate the relationship between the epicenter of the M_L6.2 Nantou earthquake and anomalous seismicity areas. Fig. 3a shows the ETAS map, or the spatial pattern of seismicity change in the prediction period for circular area centered at every calculation grid cell. To make the ETAS map, 600 events were collected for each calculation grid cell. This figure indicates the existence of significant seismic quiescence in central Taiwan including the grid cell of (121°, 24°), southeastern Taiwan including (121.4°, 23°), and northeastern Taiwan including (121.9°, 24.5°). On the other hand, a seismic activation area is also found in northwestern Taiwan. The ETAS maps obtained by applying the model to different including numbers of events (400, 600, 800, and 1000 events) are also similar in spatial pattern to one another in that the seismic quiescence regions surrounding the epicenter of the Nantou earthquake and the seismic activation area in northwestern Taiwan are clearly recognized in all the cases (not shown). This similarity implies the robustness of the spatial pattern of large seismicity change, or seismic quiescence and activation, obtained in this study.

Fig. 3b denotes the event search radius for each grid cell, within which 600 events are collected to make the ETAS map. Smaller searching radius for a grid cell reflects higher seismic activity in its surrounding area and vice versa. Fig. 3c shows the calculated p-value, which is obtained with goodness-of-fit test (two-sample Kormogorov–Smirnov (KS) test) for the target period. P-value is defined as follows:

$$Pvalue = 1 - \Pr\left(\chi^2 \le \chi_0^2\right), \tag{5}$$

where $\Pr(\chi^2 \le \chi_0^2)$ denotes the probability of χ^2 being smaller than the following KS statistics χ_0^2:

$$\chi_0^2 = 4D^2 \frac{n_1 n_2}{n_1 + n_2}, \tag{6}$$

where n_1 is actual number of earthquakes; n_2 is modeled number of earthquakes ($n_1 = n_2$); D is the maximum vertical deviation (absolute value) between the two curves showing actual and modeled cumulative relative frequencies of earthquakes ($0 \le D \le 1$).

P-value shows the goodness of model fitting to the cumulative number of events, which is classified into two categories: significant difference (poor fit) and insignificant difference (good fit); A p-value

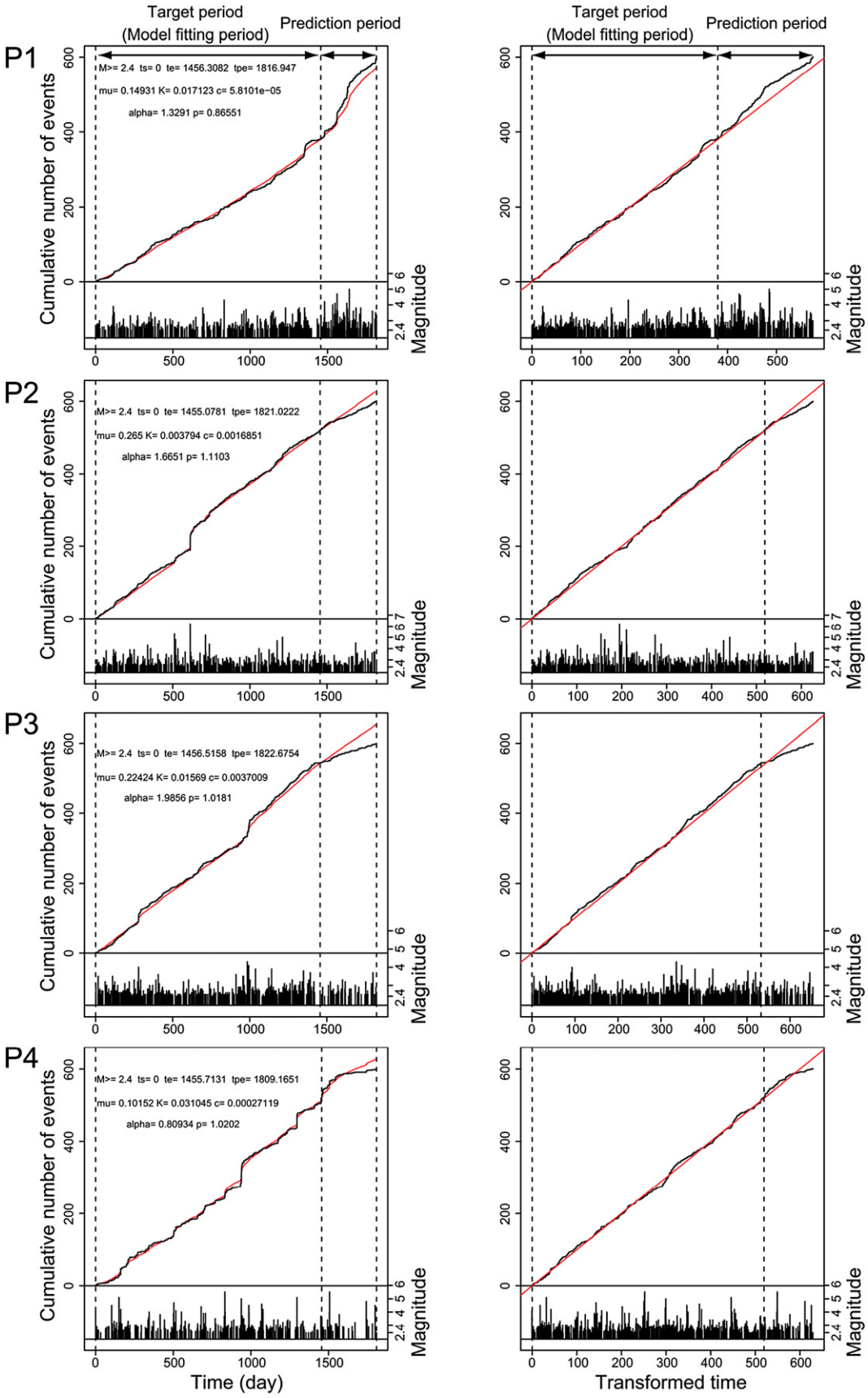

Fig. 8. As in Fig. 4, but for the target period of Mar. 1, 2008–Feb. 29, 2012 and the prediction period of Mar. 1, 2012–Feb. 28, 2013; the locations of P1 to P6 are shown in Fig. 7a.

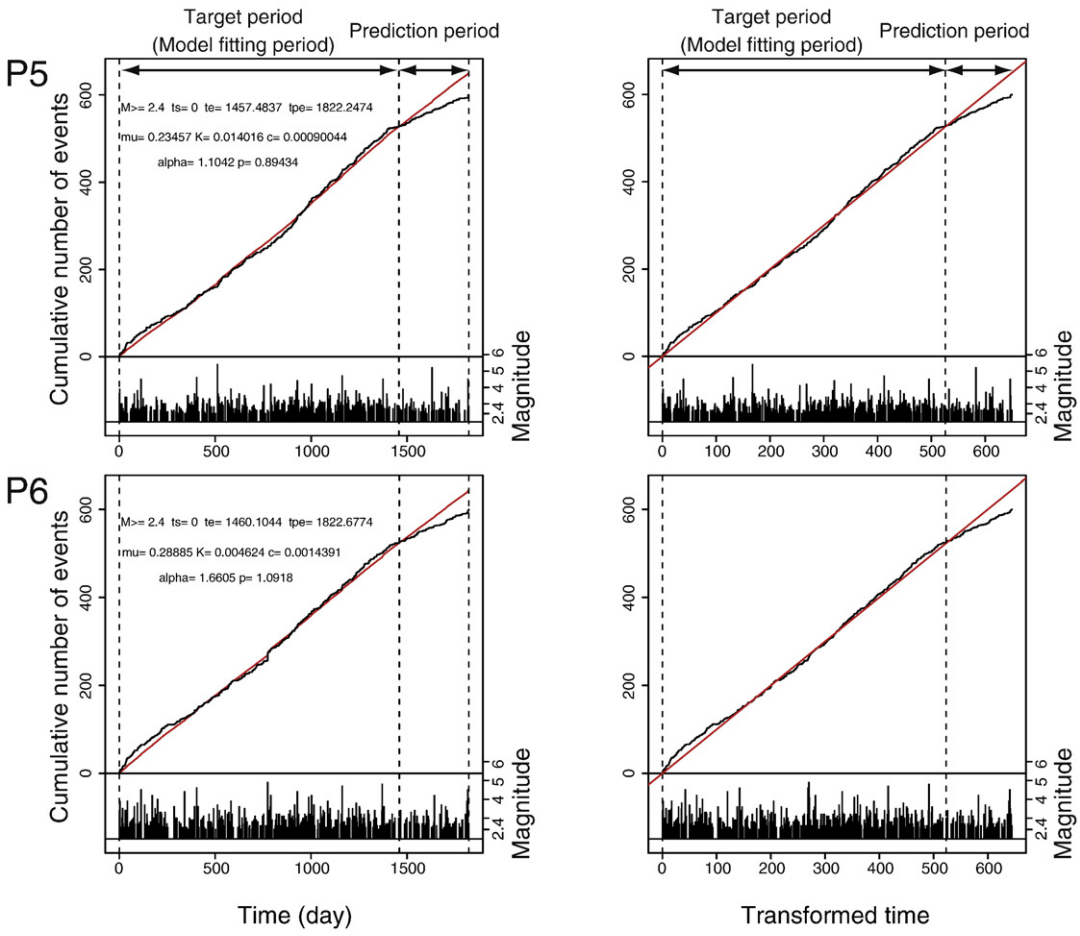

Fig. 8 (*continued*).

greater than 0.05 corresponds to a good fit. The occurrence of swarm-like events or the existence of change point(s), before and after which seismicity is characterized by different parameter values of the ETAS model, in target period often cause a poor fit of the ETAS model to the data and a part of our results is no exception especially in a part of southwestern Taiwan and a few areas off east coast of Taiwan. This problem is also discussed in Kawamura and Chen (2013) in detail.

The left and right panels of Fig. 4 show the plots of cumulative numbers of earthquakes against time in day and transformed time, respectively, for circular area centered at each calculation grid cell of P1 to P8, the locations of which are shown in Fig. 3a. As explained in Eq. (2), transformed time shows the theoretical cumulative number of earthquakes modeled by Eq. (2). Thus, the linear trend in the right panel corresponds to the seismicity distributed according to the stationary Poisson process expected from the ETAS model. The left and right panels of P1 to P3 show deviations in the prediction period upward from the straight lines, which therefore represent the occurrences of seismic activation. Contrastingly, those of P4 to P8 exhibit downward deviations from the linear trends, indicating the occurrences of seismic quiescence. Parameters t_s and t_e in the left panels correspond to the beginning and end times of the target period, respectively, which are denoted by the first two vertical dotted lines in all the panels. Parameter t_{pe} shows the end time of the prediction period, which corresponds to the last vertical dotted line in each of the left panels. Parameters of the ETAS models,μ, K, c, α and p, indicate the maximum likelihood estimates, which are obtained by fitting the ETAS model to the data for the target period (refer to Eq. (2)).

Here, we further confirmed the effect of different target and prediction periods on the existence of seismic quiescence and activation areas. Figs. 5 to 10 are the results obtained using the ETAS model for different target and prediction periods. Each pair of Figs. 5–10 correspond to the pair of Figs. 3 and 4, respectively. The target periods for Figs. 5–10 were set to Mar. 1, 2007–Feb. 29, 2012, Mar. 1, 2008–Feb. 29, 2012, and Mar. 1, 2009–Feb. 29, 2012, respectively; all of the prediction periods following the above three target periods were set as Mar. 1, 2012–Feb. 28, 2013. Intriguingly, the ETAS maps for the different target and prediction periods (Figs. 5a, 7a, and 9a) indicate that the epicenter of the 2013 M_L6.2 Nantou earthquake (Fig. 1) is surrounded by broader seismic quiescence regions and that a seismic activation area is also found in each of Figs. 5a, 7a, and 9a. It should be noted that these properties are also clearly recognized in Fig. 3a.

To further examine the robustness of the seismic quiescence and activation areas obtained, we further created two different spatial maps showing seismic quiescence and activation (Figs. 11 and 12). We here applied the PI method and the ZMAP calculation to the same CWB earthquake catalog.

Fig. 11a and b denotes the PI maps for the change intervals t_1–t_2 of Oct. 1, 2011–Sep. 30, 2012 and Mar. 1, 2012–Feb. 28, 2013, respectively. The PI map involves the information on spatiotemporally normalized seismicity rate change for each grid cell. Here, it should be noted that, because the PI method incorporates seismic quiescence and activation in data processing, discrimination between them is essentially impossible. Thus, we only know that significantly large seismicity change is representative of any one of seismic quiescence, seismic activation, and both. From Fig. 11a and b, it is recognized that the 2013 M_L6.2 Nantou earthquake occurred near the edge of significant seismicity-change areas in central Taiwan including the grid cell of (121.05°, 24.05°). It should also be noticed that each of Fig. 11a and b include a significant seismicity-change area in southeastern Taiwan including (121.45°,

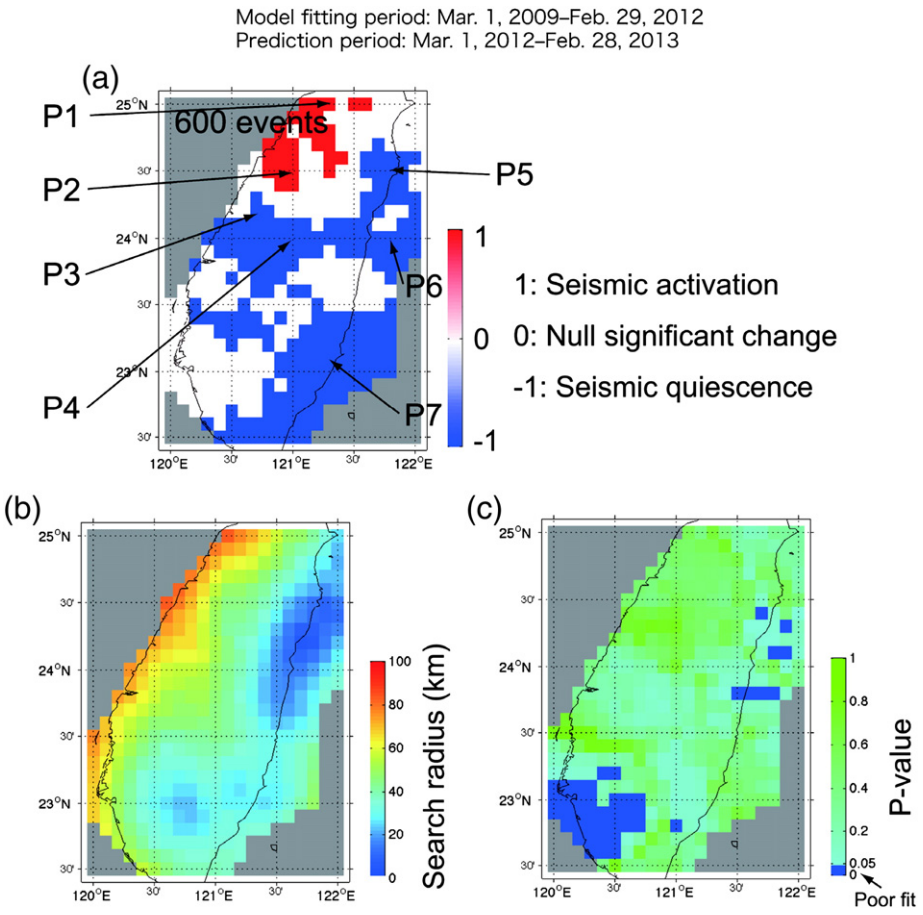

Fig. 9. As in Fig. 3, but for the target period of Mar. 1, 2009–Feb. 29, 2012 and the prediction period of Mar. 1, 2012–Feb. 28, 2013.

23.05°). Totally two main significant seismicity-change areas were identified in or near inland Taiwan region and surrounds the epicenter of the 2013 M_L6.2 Nantou earthquake; the significant seismicity-change areas are similar in location to the seismic quiescence regions recognized in the ETAS maps of Figs. 3a, 5a, 7a, and 9a. Furthermore, although smaller in scale, significant seismicity-change area(s) are also found far off the east coast of northeastern Taiwan (Fig. 11a and b) and off the northeast coast near northeastern Taiwan (Fig. 11b). In the meanwhile, there is no significant seismicity-change area that corresponds to the seismic activation area in the ETAS map of Figs. 3a, 5a, 7a, and 9a.

Fig. 12a and b shows the ZMAPs for the calculation periods of Oct. 1, 2011–Sep. 30, 2012 and Mar. 1, 2012–Feb. 28, 2013, respectively. The ZMAP represents the spatial distribution of the difference between the seismicity averaged over the calculation period and that over the background period. In making the ZMAP, to evaluate the Z value for each grid cell, only the events included in the grid cell were utilized. In Fig. 12a and b, significant seismic quiescence areas colored dark blue can be identified not only in central Taiwan including the grid cell of (121°, 24°) (region A in Fig. 12a and b), but also in southeastern Taiwan including (121.4°, 23°) (region D) and northeastern Taiwan including (121.9°, 24.5°) (region C). It should be noticed that their locations are similar to those obtained using the ETAS analysis (Figs. 3a, 5a, 7a, and 9a). Furthermore, the seismic quiescence region in northeastern Taiwan clearly extends to far off the east coast of northeastern Taiwan (region C in Fig. 12a and b). This broader seismic quiescence region including northeastern Taiwan appears to straddle the seismic quiescence region in northeastern Taiwan obtained using the ETAS model (Figs. 3a, 5a, 7a, and 9a) and a smaller area(s) with significant seismicity changes far off the east coast of northeastern Taiwan (Fig. 11a and b) and off the northeast coast near northeastern Taiwan (Fig. 11b), which were obtained using the PI method (Fig. 11a and b). In the meanwhile, a smaller seismic activation area is identified in northern Taiwan, which partially overlaps with the seismic activation area in the ETAS map of Figs. 3a, 5a, 7a, and 9a.

Summing up Figs. 3a, 5a, 7a, 9a, 11a, b, 12a, and b, the epicenter of the 2013 M_L6.2 Nantou earthquake is surrounded by the seismic quiescence regions in central Taiwan, southeastern Taiwan, and northeastern Taiwan. The seismic quiescence or significant seismicity-change regions for central and southeastern Taiwan are found in all of the ETAS maps, PI maps, and ZMAPs (Figs. 3a, 5a, 7a, 9a, 11a, b, 12a, and b). In the meanwhile, that for northeastern Taiwan is clearly recognized in the ETAS maps and ZMAPs (Figs. 3a, 5a, 7a, 9a, 12a, and b). It is also intriguing that seismic activation areas are found in Figs. 3a, 5a, 7a, 9a, and 12a. However, the corresponding areas in Fig. 11a and b are not identified as seismic activation and large seismicity change. This issue is discussed in Section 4.

4. Discussion and conclusions

We applied the ETAS model to the earthquake catalog of Taiwan region prior to the 2013 M_L6.2 Nantou earthquake. We found that its epicenter was surrounded by three main regions with seismic quiescence or large seismicity changes, which were located in central, southeastern, and northeastern Taiwan regions as shown in Figs. 3a, 5a, 7a, and 9a. We also identified a seismic activation area in northern Taiwan in Figs. 3a, 5a, 7a, and 9a. To enhance the reliability of the spatial distribution of seismic quiescence and activation obtained using the ETAS model, we further applied the PI method and the ZMAP analysis to the same catalog of CWB. Each of the anomalous seismicity regions in central and southeastern regions is similar in location between the three different maps. This implies the robustness of the occurrences of seismic

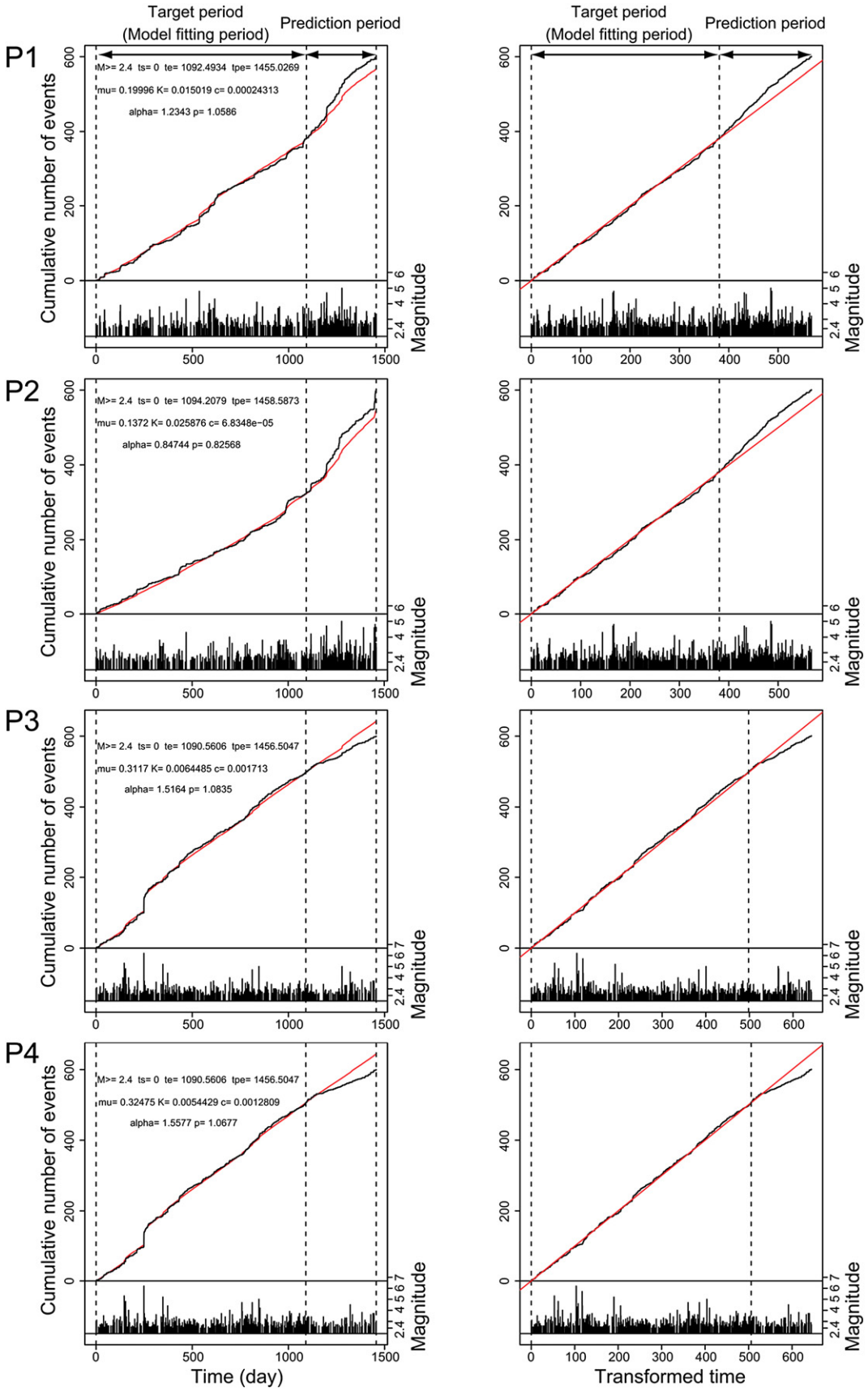

Fig. 10. As in Fig. 4, but for the target period of Mar. 1, 2009–Feb. 29, 2012 and the prediction period of Mar. 1, 2012–Feb. 28, 2013; the locations of P1 to P7 are shown in Fig. 9a.

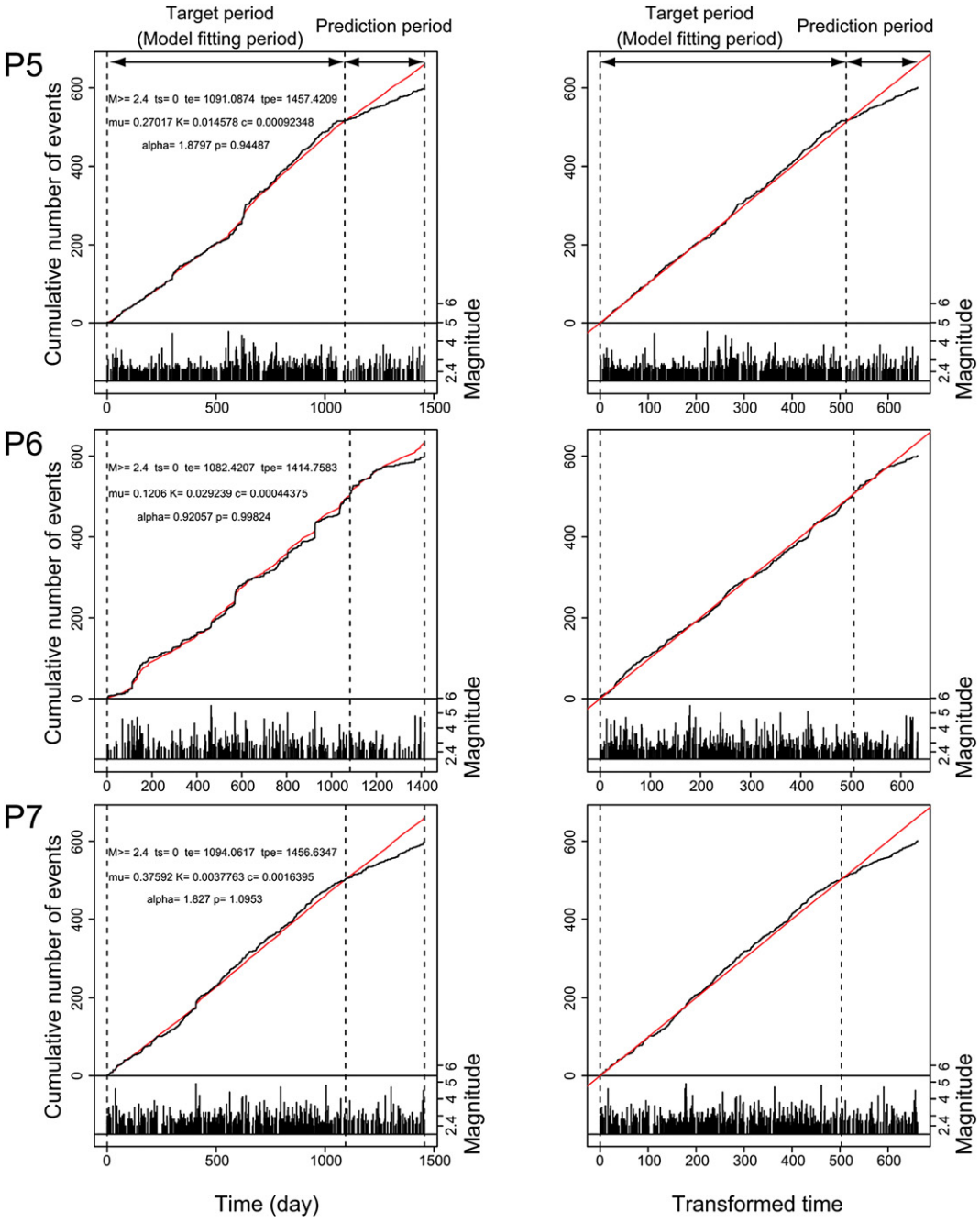

Fig. 10 (*continued*).

quiescence in central and southeastern regions. The reliability is also supported by the similarity between the ETAS maps obtained by applying the ETAS model to different including numbers of events (400, 600, 800, and 1000 events) (not shown). Although the seismic quiescence region in northeastern Taiwan obtained using the ETAS model (Figs. 3a, 5a, 7a, and 9a) and the significant seismicity-change area(s) off the east coast of northeastern Taiwan obtained using the PI method (Fig. 11a and b) are not overlapped, the broader seismic quiescence region in northeastern Taiwan obtained using the ZMAP method (region C in Fig. 12a and b) straddles them. Therefore, the existence of the seismic quiescence region in northeastern Taiwan would be reliable. The characteristic of the ETAS map that the source area of the M_L6.2 Nantou earthquake is surrounded by the broader seismic quiescence regions is quite consistent with those of the ZMAP method (Wu and Chen, 2007; Wu and Chiao, 2006) and the ETAS model (Kawamura and Chen, 2013) which is obtained for the 1999 Chi-Chi, Taiwan earthquake.

We here indicate the occurrence mechanism of seismic quiescence over broader regions surrounding the epicenter of the M_L6.2 Nantou earthquake would be due to a precursory slip on its fault plane or its deeper extent. Ogata (2005, 2011) showed the coincidence of precursory seismic activation and quiescence areas with the spatial distribution of positive and negative Coulomb failure stress changes, respectively, for the 2003 earthquake in Northern Miyagi prefecture (M6.4 (based on the magnitude scale of Japan Meteorological Agency)), the 2007 Noto Hanto earthquake (M6.9), and the 2007 Niigataken Chuetsu-oki earthquake (M6.8) in Japan. By a numerical simulation using rate- and state-dependent friction laws (Ruina, 1983), Kato et al. (1997) demonstrated that the appearance of seismic quiescence in continental crust

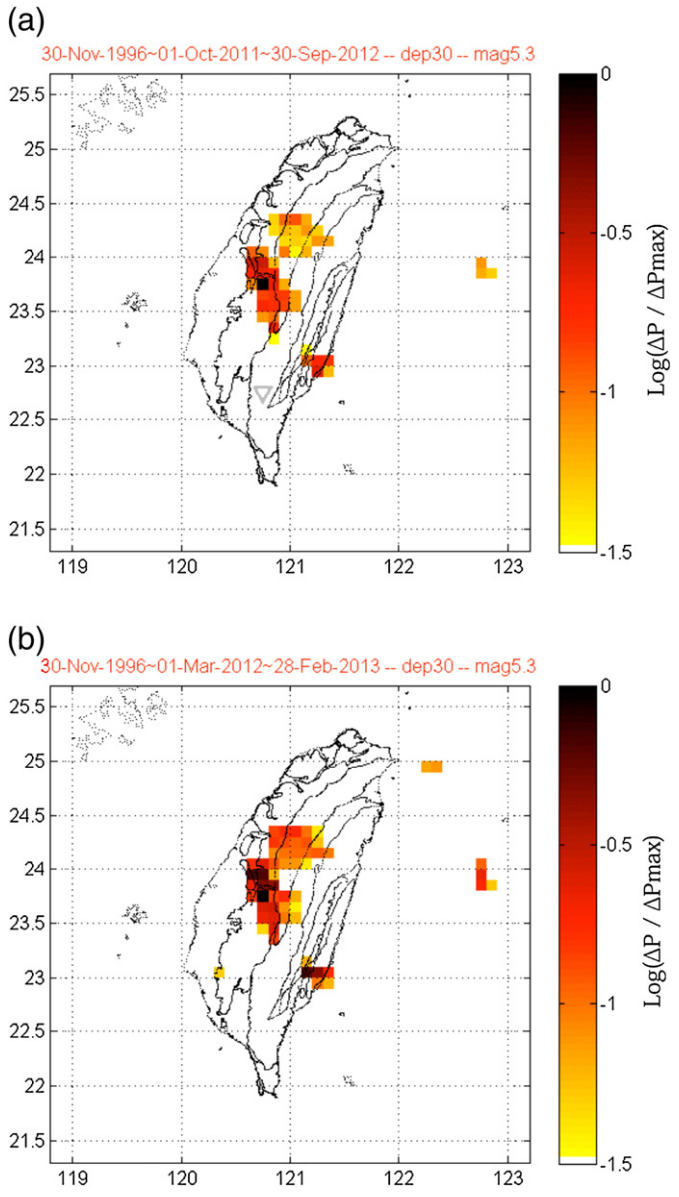

Fig. 11. PI maps, or the spatial distributions of anomalous seismicity obtained using the PI method, for the change intervals t_1–t_2 of (a) Oct. 1, 2011–Sep. 30, 2012 and (b) Mar. 1, 2012–Feb. 28, 2013. Grid cells colored warmer represent higher probabilities of earthquake occurrence after the change interval and those colored red correspond to the highest probability.

over a wider region than a source area before a large interplate earthquake is due to the regional stress relaxation which is caused by preseismic sliding on a boundary between a subducting oceanic plate and the overriding continental plate. According to their argument, the mechanism of the seismic quiescence can also be applied to other types of earthquakes, such as intraplate earthquakes on active faults. Kawamura and Chen (2013) obtained the spatial pattern of seismic activation near the source area of the Chi-Chi earthquake and seismic quiescence surrounding the seismic activation areas prior to the occurrence of the earthquake. They interpreted the possible occurrence mechanism of seismic quiescence over broader regions prior to the Chi-Chi earthquake as due to preseismic sliding on its fault plane, which is also supported by precursory abnormal strain rate change obtained using geodetic data of Taiwan GPS network (Hou et al., 2003). According to Kawamura and Chen (2013), not only the emergence of broader seismic quiescence regions but also seismic activation areas near the source area of the Chi-Chi earthquake seems to be an important characteristic of seismicity pattern which would be caused by a preseismic sliding on its fault plane (Kawamura and Chen, 2013; Wu and Chiao, 2006). It should be noted that there is a similarity between the 1999 Chi-Chi earthquake and the 2013 M_L6.2 Nantou earthquake in that seismic quiescence emerged over broader regions around the source areas of those earthquakes. However, it should also be noticed that there is a difference between the two earthquakes in that seismic activation appeared near the source area of the Chi-Chi earthquake while it did not emerge near that of the M_L6.2 Nantou earthquake. This difference may be due to the fact that the magnitude of the M_L6.2 Nantou earthquake is smaller than that of the Chi-Chi earthquake (M_L7.3). In addition, the depth of the M_L6.2 Nantou earthquake (15.4 km) is nearly twice deeper than that of the Chi-Chi earthquake, which also possibly makes it difficult to detect seismic activation near the source area of the M_L6.2 Nantou earthquake. Therefore, seismic quiescence obtained in the present study would be associated with the regional stress relaxation prior to the M_L6.2 Nantou earthquake.

It is also recognized that there exists a seismic activation area in northern Taiwan, which is denoted in Figs. 3a (P1 to P3), 5a (P1 and P2), 7a (P1), and 9a (P1 and P2), and 12 while it was not identified in Fig. 11. The physical mechanism for causing this difference is not unclear. However, it would reflect that the seismic activation is significant but is not so much as the seismic quiescence is. Because there is an instance in which seismic activation emerged prior to the Chi-Chi earthquake near its source area (Kawamura and Chen, 2013; Wu and Chiao, 2006), the possibility of the occurrence of preseismic sliding on the fault plane of a future M7-class large earthquake in the seismic activation area should be taken into account. The seismic activation may emerge also in the PI map in the near future. Therefore, we should continue to monitor the temporal variations in seismicity and strain rate in northern Taiwan.

We conclude that the emergence of seismic quiescence over broader regions surrounding the source area of the 2013 M_L6.2 Nantou earthquake obtained using three different approaches of the ETAS model, the PI method, and the ZMAP analysis supports the hypothesis that it was caused by preseismic sliding on the fault plane or its deeper extension of the earthquake. The spatial distributions of seismic quiescence and activation obtained using the PI method and the ZMAP method enhance the reliability of the ETAS map and therefore the hypothesis of preseimic sliding. The result in which seismic activation near the source area of the M_L6.2 Nantou earthquake were not identified may be related to the fact that its magnitude and depth are smaller ($M_L < 7$) and deeper than those of the Chi-Chi earthquake, respectively.

Acknowledgments

An anonymous reviewer's suggestions were useful for improving the manuscript. The authors used the earthquake catalog maintained by the Central Weather Bureau, Taiwan. We thank the staffs for maintaining the catalog. This research was supported by the Ministry of Science and Technology of the Republic of China (102-2811-M-002-064).

Appendix A

The statistical tests utilized for assessing the occurrence of anomalous seismicity change in the ETAS analysis (Section 2.1) are as follows. The reader can also refer to the detailed flowchart (Fig. 1) of Kawamura and Chen (2013).

a) The first test assesses the significance of change in mean difference between modeled and actual cumulative numbers of earthquakes before and after the middle of the prediction period. The purpose of this test is to investigate the existence of anomalous seismicity especially in the latter half of the prediction period rather than the first half. For example, if the deviation of actual seismicity from

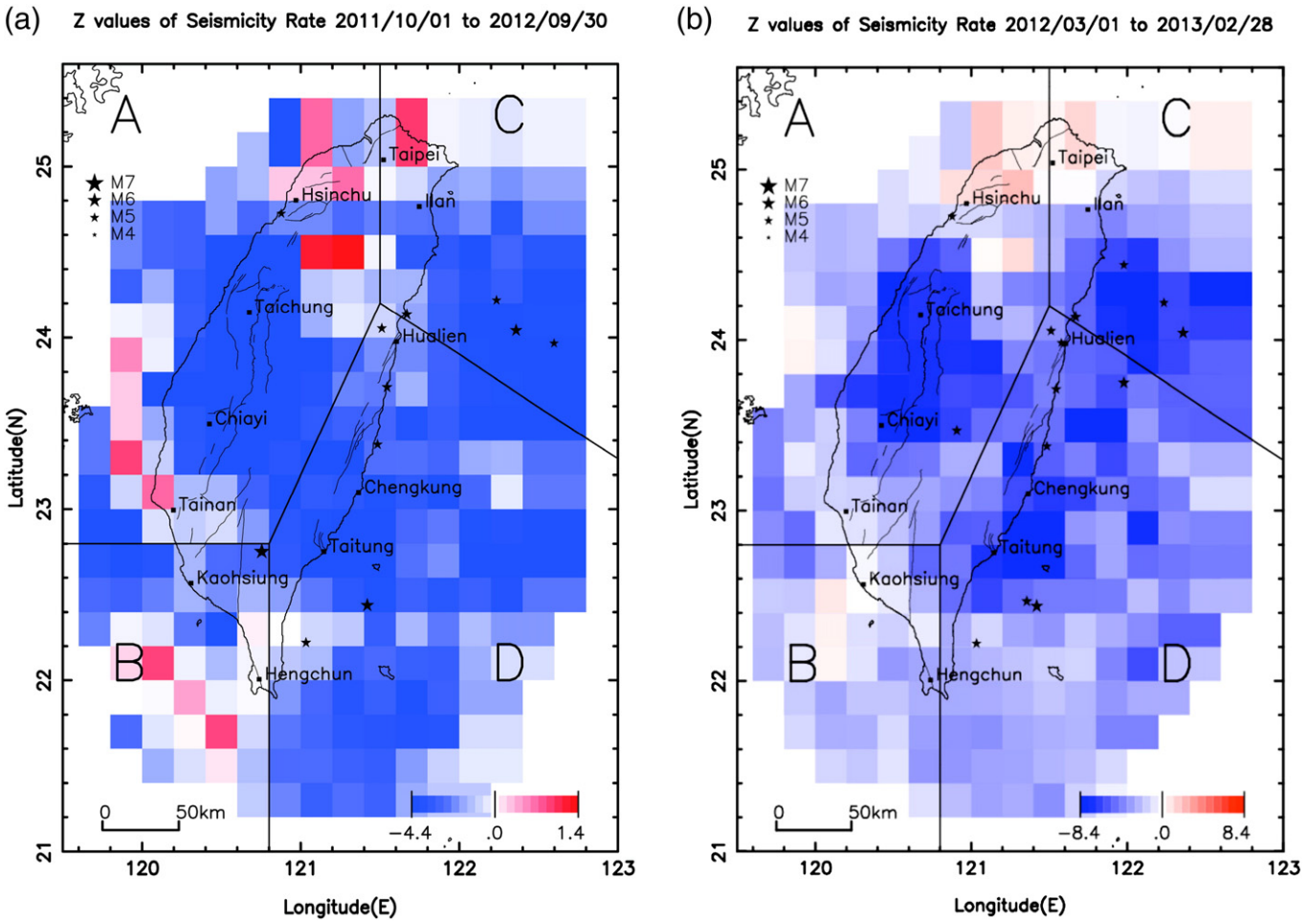

Fig. 12. ZMAPs, or the spatial distributions of seismicy changes obtained using the ZMAP analysis (blue color: seismic quiescence, red color: seismic activation, and white color: null significant change), for the calculation periods of (a) Oct. 1, 2011–Sep. 30, 2012 and (b) Mar. 1, 2012–Feb. 28, 2013. Grid cells colored darker denote more significant seismicity change.

theoretical one is larger in the latter half of the prediction period than in the first half, the statistical test leads to the judgment that abnormal seismicity continues up to the end of the prediction period. In the modeled seismicity, the sequence of transformed times is distributed according to the stationary Poisson process (Brown et al., 2001; Papangelou, 1972). In the statistical test, the prediction period is evenly divided into two transformed-time intervals and the following statistics is calculated for the i-th grid cell:

$$Z_{iA} = (R_{i1} - R_{i2}) \Big/ \sqrt{\frac{\sigma_{i1}^2}{n_{i1}} + \frac{\sigma_{i2}^2}{n_{i2}}}, \tag{A.1}$$

where R_{i1} and R_{i2} are the mean differences between modeled and actual cumulative earthquake numbers for the first half and the latter half transformed-time intervals, respectively; n_{i1} and n_{i2} are the numbers of earthquakes for respective transformed-time intervals; σ_{i1} and σ_{i2} are standard deviations of differences between modeled and actual cumulative earthquake numbers for respective transformed-time intervals. If Z_{iA} is significantly positive, then the seismicity change is regarded as seismic quiescence; If Z_{iA} is significantly negative, it is regarded as seismic activation; If Z_{iA} is not significant, it is not regarded as anomalous seismicity. Final judgment and classification of seismicity for the prediction period for each grid cell depends on the result of the following second test.

b) The second test assesses the significance of difference between the numbers of local transformed-time windows for seismic quiescence and seismic activation in the prediction period. The purpose of this test is to investigate the existence of seismic quiescence or seismic activation for each local transformed-time window in the prediction period. Seismicity for the k-th local transformed-time window for the i-th grid cell $(\tau_{ik} - h, \tau_{ik})$ in the prediction period is classified into three patterns: seismic quiescence, seismic activation, and null significant change; parameter h represents the width of transformed-time window; The local transformed-time window is moved forward by a constant interval, i.e. 0.25 h. To classify seismicity in each local transformed-time window into the three patterns, we evaluated the significance of difference between the actual cumulative number of earthquakes and the modeled one that is calculated from the ETAS model. For example, if the number of local transformed-time windows for seismic quiescence is significantly more than that for seismic activation, the statistical test leads to the judgment that seismic quiescence is prominent in the prediction period. Here, for convenience of assessing the significance of difference, the number of events for the i-th grid cell and the k-th local transformed-time window in the prediction period $(\tau_{ik} - h, \tau_{ik})$, ΔN_{ik}, is transformed to a variable ξ_{ik} that is approximately distributed according to a normal distribution with mean 0 and variance 1 by the following equation (Ogata, 1988; Shimizu and Yuasa, 1984),

$$\begin{aligned}\xi_{ik} &= \xi_{ik}(\Delta N_{ik}, h) \\ &= \frac{33\Delta N_{ik} + 29 - h - (32\Delta N_{ik} + 31)[h/(\Delta N_{ik} + 1)]^{1/4}}{9(\Delta N_{ik} + 1)^{1/2}}.\end{aligned} \tag{A.2}$$

When $\xi > 2$, seismic activation is assessed as predominant in the local transformed-time window. Conversely, when $\xi < -2$, seismic quiescence is regarded as predominant. The case of $-2 \le \xi \le 2$ indicates null significant change of seismicity in the prediction period. The criteria are based on panels 3a and 3b of Fig. 15 in Ogata (1988). After counting the numbers of local transformed-time windows for seismic quiescence and seismic activation based on Eq. (A.2) for the i-th grid cell, the significance of difference between their counts is evaluated by the following equation:.

$$Z_{iB} = \left(p_{iq} - p_{ia}\right) \Big/ \sqrt{\left\{\left(p_{iq} + p_{ia}\right) - \left(p_{iq} - p_{ia}\right)^2\right\} \Big/ n_{iall}}, \tag{A.3}$$

where p_q and p_a are the numbers of local transformed-time windows for seismic quiescence and seismic activation, respectively, which are normalized by the total number of local transformed-time windows n_{all} in the prediction period. If Z_{iB} is significantly positive, then the seismicity change is regarded as seismic quiescence; If Z_{iB} is significantly negative, it is regarded as seismic activation; If Z_{iB} is not significant, it is not regarded as anomalous seismicity.

When both of these statistical tests a) and b) are assessed as significant and the signs of Z_{iA} and Z_{iB} are the same, seismicity is regarded as seismic quiescence (positive sign) or seismic activation (negative sign). Based on the significances and signs of Z_{iA} and Z_{iB}, the temporal change in seismicity for the prediction period for the i-th grid cell is then categorized into the three types: seismic activation, seismic quiescence, and null significant change. If both Z_{iA} and Z_{iB} are positive and significantly large, then the seismicity change is regarded as seismic quiescence; If both Z_{iA} and Z_{iB} are negative and significantly large, then it is assessed as seismic activation; If at least one of Z_{iA} and Z_{iB} is not significantly large or Z_{iA} and Z_{iB} are significantly large but have different signs, it is not regarded as anomalous seismicity.

References

Bansal, A.R., Ogata, Y., 2013. A non-stationary epidemic type aftershock sequence model for seismicity prior to the December 26, 2004 *M* 9.1 Sumatra–Andaman mega-earthquake. J. Geophys. Res. 118, 616–629.

Bowman, D.D., King, G.C.P., 2001. Accelerating seismicity and stress accumulation before large earthquakes. Geophys. Res. Lett. 28, 4039–4042.

Bowman, D.D., Ouillon, G., Sammis, G., Sornette, A., Sornette, D., 1998. An observed test of the critical earthquake concept. J. Geophys. Res. 103, 24359–24372.

Brown, E.N., Barbieri, R., Ventura, V., Kass, R.E., Frank, L.M., 2001. The time-rescaling theorem and its application to neural spike train data analysis. Neural Comput. 14, 325–346.

Bufe, C.G., Varnes, D.J., 1993. Predictive modeling of the seismic cycle of the greater San Francisco Bay region. J. Geophys. Res. 98 (9871–9883), 1993.

Bufe, C.G., Nishenko, S.P., Varnes, D.J., 1994. Seismicity trends and potential for large earthquakes in the Alaska-Aleutian region. Pure Appl. Geophys. 142, 83–99.

Central Geological Survey, 2010. Active fault map of Taiwan. available at http://fault.moeacgs.gov.tw/TaiwanFaults_2009/News/NewsView.aspx?id=3.

Chen, C.C., 2003. Accelerating seismicity of moderate-size earthquakes before the 1999 Chi-Chi, Taiwan, earthquake: testing time-prediction of the self-organizing spinodal model of earthquakes. Geophys. J. Int. 155, F1–F5.

Chen, C.C., Rundle, J.B., Holliday, R., Nanjo, K.Z., Turcotte, D.L., Li, S.C., Tiampo, K.F., 2005. The 1999 Chi-Chi, Taiwan, earthquake as a typical example of seismic activation and quiescence. Geophys. Res. Lett. 32, L22315. http://dx.doi.org/10.1029/2005GL023991.

Chen, C.C., Rundle, J.B., Li, H.C., Holliday, J.R., Nanjo, K.Z., Turcotte, D.L., Tiampo, K.F., 2006. From tornadoes to earthquakes: forecast verification for binary events applied to the 1999 Chi-Chi, Taiwan, earthquake. Terr. Atmos. Ocean. Sci. 17, 503–516.

Chuang, R.Y., Johnson, K.M., Wu, Y.M., Ching, K.E., Kuo, L.C., 2013. A midcrustal ramp-fault structure beneath the Taiwan tectonic wedge illuminated by the 2013 Nantou earthquake series. Geophys. Res. Lett. 40, 5080–5084.

Console, R., Montuori, C., Murru, M., 2000. Statistical assessment of seismicity patterns in Italy: are they precursors of subsequent events? J. Seismol. 4, 435–449.

Habermann, R.E., 1988. Precursory seismic quiescence: past, present, and future. Pure Appl. Geophys. 126, 279–318.

Habermann, R.E., Wyss, M., 1984. Earthquake triggering during preparation for great earthquakes. Geophys. Res. Lett. 11, 291–294.

Holliday, J.R., Nanjo, K.Z., Tiampo, K.F., Rundle, J.B., Turcotte, D.L., Donnellan, A., 2005. Forecasting the locations of future earthquake and its verification. Nonlinear Process. Geophys. 12, 965–977.

Holliday, J.R., Rundle, J.B., Tiampo, K.F., Klein, W., Donnellan, A., 2006. Systematic procedural and sensitivity analysis of the pattern informatics method for forecasting large ($M \ge 5$) earthquake events in southern California. Pure Appl. Geophys. 12, 965–977.

Hou, C., Chen, Y., Hu, J., Lin, C., Yu, S., Chen, C., Wang, J., 2003. Feasibility study on earthquake precursor using GPS data in Taiwan. American Geophysical Union, Fall Meeting 2003, abstract #T12C-0478.

Jaume, S.C., Sykes, L.R., 1999. Evolving towards a circular point: a review of accelerating seismic moment/energy release prior to large and great earthquakes. Pure Appl. Geophys. 155, 279–306.

Karakaisis, G.F., Papazachos, C.B., Savvaidis, A.S., Papazachos, B.C., 2002. Accelerating seismic crustal deformation in the North Aegean Trough, Greece. Geophys. J. Int. 148, 193–200.

Kato, N., Ohtake, M., Hirasawa, T., 1997. Possible mechanism of precursory seismic quiescence: regional stress relaxation due to preseismic sliding. Pure Appl. Geophys. 150, 249–267.

Katsumata, K., 2011. A long-term seismic quiescence started 23 years before the 2011 off the Pacific coast of Tohoku Earthquake ($M = 9.0$). Earth Planets Space 63, 709–712.

Kawamura, M., Chen, C.-C., 2013. Precursory change in seismicity revealed by the Epidemic-Type Aftershock-Sequences model: a case study of the 1999 Chi-Chi, Taiwan earthquake. Tectonophysics 592, 141–149.

Kawamura, M., Wu, Y.-H., Kudo, T., Chen, C.-C., 2013. Precursory migration of anomalous seismic activity revealed by the pattern informatics method: a case study of the 2011 Tohoku earthquake, Japan. Bull. Seismol. Soc. Am. 103 (2B), 1171–1180.

Kawamura, M., Wu, Y.-H., Kudo, T., Chen, C.-C., 2014. A statistical feature of anomalous seismic activity prior to large shallow earthquakes in Japan revealed by the pattern informatics method. Nat. Hazards Earth Syst. Sci. 14, 849–859.

Ma, K.-F., Chan, C.-H., Stein, R.S., 2005. Response of seismicity to Coulomb stress triggers and shadows of the 1999 Mw = 7.6 Chi-Chi, Taiwan, earthquake. J. Geophys. Res. 110, B05S19. http://dx.doi.org/10.1029/2004JB003389.

Mignan, A., Werner, M.J., Wiemer, S., Chen, C.-C., 2011. Bayesian estimation of the spatially varying completeness magnitude of earthquake catalogs. Bull. Seismol. Soc. Am. 101, 1371–1385.

Mogi, K., 1969. Some features of recent seismic activity in and near Japan (2). Bull. Earthq. Res. Inst. 46, 30–36.

Ogata, Y., 1988. Statistical models for eathquake occurrences and residual analysis for point processes. J. Am. Stat. Assoc. 83 (401), 9–27.

Ogata, Y., 1992. Detection of precursory relative quiescence before great earthquakes through a statistical model. J. Geophys. Res. 97, 19845–19871.

Ogata, Y., 1999. Seismicity analysis through point-process modeling: a review. Pure Appl. Geophys. 155, 471–507.

Ogata, Y., 2005. Detection of anomalous seismicity as a stress change sensor. J. Geophys. Res. 110, B05S06. http://dx.doi.org/10.1029/2004JB003245.

Ogata, Y., 2011. Pre-seismic anomalies in seismicity and crustal deformation: case studies of the 2007 Noto Hanto earthquake of M6.9 and the 2007 Chuetsu-oki earthquake of M6.8 after the 2004 Chuetsu earthquake of M6.8. Geophys. J. Int. 186, 331–348.

Papangelou, F., 1972. Integrability of expected increments of point processes and a related random change of scale. Trans. Am. Math. Soc. 165, 483–506.

Papazachos, B.C., Karakaisis, G.F., Scordilis, E.M., Papazachos, C.B., Panagiotopoulos, D.G., 2010. Present patterns of decelerating-accelerating seismic strain in South Japan. J. Seismol. 14. http://dx.doi.org/10.1007/s10950-009-9165-z.

Resenberg, P.A., Matthews, M.V., 1988. Precursory seismic quiescence: a preliminary assessment of the hypothesis. Pure Appl. Geophys. 126, 373–406.

Ruina, A.L., 1983. Slip instability and state variable friction laws. J. Geophys. Res. 88, 10359–10370.

Rundle, J.B., Klein, W., Tiampo, K., Gross, S., 2000. Linear pattern dynamics in nonlinear threshold systems. Phys. Rev. E. 61, 2418–2431.

Shimizu, R., Yuasa, M., 1984. Normal approximation for asymmetric distributions. Proc. Inst. Stat. Math. 32, 141–158.

Stein, R.S., 1999. The role of stress transfer in earthquake occurrence. Nature 402, 605–609.

Sykes, L.R., Jaume, S.C., 1990. Seismic activity on neighboring faults as a long-term precursor to large earthquakes in the San Francisco Bay area. Nature 348, 595–599.

Tiampo, K.F., Rundle, J.B., McGinnis, S., Gross, S.J., Klein, W., 2002a. Mean-field threshold systems and phase dynamics: an application to earthquake fault systems. Europhys. Lett. 60, 481–487.

Tiampo, K.F., Rundle, J.B., McGinnis, S., Gross, S.J., Klein, W., 2002b. Eigenpatterns in southern California seismicity. J. Geophys. Res. 107 (B12), 2354. http://dx.doi.org/10.1029/2001JB000562.

Toda, S., Stein, R.S., Sagiya, T., 2002. Evidence from the A.D. 2000 Izu islands earthquake swarm that stressing rate governs seismicity. Nature 419, 58–61.

Wiemer, S., Wyss, M., 1994. Seismic quiescence before the Landers ($M = 7.5$) and Big Bear ($M = 6.5$) 1992 earthquakes. Bull. Seismol. Soc. Am. 84, 900–916.

Wiemer, S., Wyss, M., 2000. Minimum magnitude of completeness in earthquake catalogs: examples from Alaska, the western United States, and Japan. Bull. Seismol. Soc. Am. 90, 859–869.

Wu, Y.M., Chen, C.C., 2007. Seismic reversal pattern for the 1999 Chi-Chi, Taiwan, Mw7.6 earthquake. Tectonophysics 429, 125–132.

Wu, Y.M., Chiao, L.Y., 2006. Seismic quiescence before the 1999 Chi-Chi, Taiwan, Mw7.6 earthquake. Bull. Seism. Soc. Am. 96, 321–327.

Wu, Y.H., Chen, C.C., Rundle, J.B., 2008a. Detecting precursory earthquake migration patterns using the pattern informatics method. Geophys. Res. Lett. 35, L19304. http://dx.doi.org/10.1029/2008GL035215.

Wu, Y.M., Chen, C.C., Zhao, Li, Chang, C.H., 2008b. Seismicity characteristics before the 2003 Chengkung, Taiwan, earthquake. Tectonophysics 457, 177–182.

Wu, Y.H., Chen, C.C., Rundle, J.B., 2011. Precursory small earthquake migration patterns. Terra Nova 23, 369–374.

Wyss, M., Wiemer, S., 1997. Two current seismic quiescences within 40 km of Tokyo. Geophys. J. Int. 128, 459–473.